Nonlinear Virtual Inertia Control of WTGs for Enhancing Primary Frequency Response and Suppressing Drivetrain Torsional Oscillations

Bi Liu, Junbo Zhao, *Senior Member, IEEE*, Qi Huang, *Senior Member, IEEE*, Federico Milano, *Fellow, IEEE*, Yingchen Zhang *Senior Member, IEEE*

***Abstract*—Virtual inertia controllers (VICs) for wind turbine generators (WTGs) have been recently developed to compensate the reduction of inertia in power systems. However, VICs can induce drivetrain torsional oscillations of WTGs. This paper addresses this issue and develops a novel nonlinear VIC based on objective holographic feedback theory and the definition of a completely controllable system of Brunovsky type. Simulation results under various scenarios demonstrate that the proposed technique outperforms existing VICs in terms of enhancement of system frequency nadir, suppression of WTG drivetrain torsional oscillations, fast and smooth recovery of WTG rotor speed to the original maximum power point (MPP) before the disturbance as well as preventing secondary frequency dip caused by traditional VIC. The proposed technique is also able to adaptively coordinate multiple WTGs to enhance the frequency support and the dynamic perfomance of each WTG.**

***Index Terms*—Wind generation, frequency control, virtual inertia control, torsional oscillations, power system stability.**

I. Introduction

The increasing penetration of variable-speed wind turbine generators (WTGs) results in a reduction of system inertia, which deteriorates the primary frequency response [1]. To this end, some utilities have updated their grid codes and start to leverage WTGs for primary frequency support [2]–[4]. Two strategies have been widely used, namely the wind power deloading based VIC and MPP tracing-based VIC.

For the first type of VIC, the wind turbines do not supply the maximum available power in normal situation, and thus a wind power margin can be maintained for grid frequency support. By de-loading WTGs and changing its reference electromagnetic power as a function of grid frequency deviation, the supplementary control on WTG [5] provides grid frequency support. Rotor speed control and pitch angle control enable WTGs to reserve sufficient active power as a necessary auxiliary of grid frequency regulation [6], [7]. In [8], the frequency-droop scheme for WTG is developed by acting on the blade pitch angle to preserve a power reserve margin for primary frequency regulation. Although being effective, de-loading leads to the economic loss of wind farm owners.

To deal with that, the MPP tracing-based VIC is proposed by changing WTG active power set point with the MPP tracing curve. Changing the doubly-fed induction generator (DFIG) torque set point based on the derivative of frequency deviation [9], [10] introduces inertial response to the grid frequency event through the provisional release of rotor kinetic energy of WTG. For example, [11]–[13] adopt a function of the frequency deviation and derivative of frequency deviation as the additional torque set point of WTG to couple WTG rotor speed with the grid frequency, which increases kinetic energy discharge capability. Combining the WTG inertial control with pitch angle control allows WTG to participate in restoring grid frequency after a disturbance [14]. However, a predetermined fixed gain needs to be defined. A large gain ensures an improved frequency nadir, but it might cause over-deceleration of the WTG rotor speed, especially in presence of low wind speed; by contrast, a small gain may waste the kinetic energy of WGT rotor under high wind speed situation, thus decreasing the frequency support capability. Moreover, to restore WTG rotor speed, VIC with fixed parameters can only operate at a preset period and this may cause secondary frequency drop due to the instant reduction of WTG electromagnetic power [15], [16]. As shown in [17]–[19], the frequency response strongly depends on the operating points of WTG, and therefore the VIC parameters should be tuned accordingly.

By continuously adjusting the droop coefficient of WTG VIC in response to wind velocities, the primary frequency response from the deloaded WTGs on the basis of the available margin is significantly improved [19], [21]. VIC developed in [22] adjusts the gain of frequency deviation based on the maximum frequency deviation. This scheme can indeed enhance the frequency nadir and release kinetic energy of WTG rotor during the initial stage of the event, but it might still cause the over-deceleration of rotor speed, especially in presence of low wind speed. In fact, this controller has no ability of automatically evaluating the available kinetic energy stored in WTG rotor. In [23], the derivative of frequency deviation is used to emulate the exact inertial response of DFIG. The gain of the derivative is varied proportionally to the DFIG operating rotor speed, thus avoiding the over-deceleration of rotor speed. Furthermore, [24] proposes a VIC strategy to formulate the inertia constant and primary power

This research work is supported by The National Key Research and Development Program of China (No. 2017YFB0902002).

B. Liu and Q. Huang are with the Sichuan Provincial Key Lab of Power System Wide-area Measurement and Control, University of Electronic Science and Technology of China, Chengdu, Sichuan, 611731, PR China. (e-mail: liubi_2006@126.com; whu@uestc.edu.cn).

J. Zhao is with the Department of Electrical and Computer Engineering, Mississippi State University, Starkville, MS 39762, (junbo@ece.msstate.edu).

F. Milano is with the School of Electrical and Electronic Engineering, University College Dublin, Dublin, Ireland (e-mail: federico.milano@ucd.ie).

Y. Zhang is with National Renewable Energy Laboratory, Golden, CO 80401 USA (e-mail: Yingchen.Zhang@nrel.gov).

reserve of WTG that operates at derated power conditions. These formulations are leveraged to evaluate the capability of providing primary frequency support power from a wind farm using an aggregated wind speed.

In [25], the output of VIC is determined as the product of the frequency deviation and adaptive gain, which is set to be high during the early stage of a disturbance, when the derivative of frequency derivation and rotor speed are high. When the frequency nadir is reached, the gain is decreased. Nevertheless, since WTGs absorb the active power from grid during the rotor speed recovery, the inertial response of WTGs is even worse than the condition under which WTGs do not participate in the response of grid frequency. To this end, [26] suggests the parameters of VIC to be determined by the stored kinetic energy of WTG rotor and the captured wind power. However, [27] indicates that VIC deteriorates the drive-train torsional oscillation of WTG, which has not been taken into consideration in the aforementioned VICs. Since the frequency control strengthens coupling between grid frequency and rotor speed of the WTG, disturbances of grid frequency leads to the deviation of WTG rotor speed from the MPP [28].

In [29]–[31], damping controllers are designed to suppress the torsional oscillation of WTG drive train. [29] investigates the band-pass filters for torsional oscillation control and the damping is achieved through pole placement using state feedback. In [31], by introducing a damping torque component, an auxiliary active damping control known as wind turbine stabilizer is proposed to improve the damping ratio of the torsional oscillatory modes. However, these studies concentrate on the damping of WTG drivetrain without VIC. By integrating multiple active damping loops into the active and reactive controller of WTG, the impact of VIC on drivetrain torsional oscillation is mitigated [32]. Reference [33] modulates the reactive power to counteract WTG torsional oscillation impacted by VIC.

It is worth pointing out that the design of new VIC while maintaining the capability of suppressing the drivetrain torsional oscillation of WTG is challenging. Besides, how to adaptively coordinate the frequency support power among WTGs with different operating points is another important open problem.

A. Contributions

To address the aforementioned challenges, this paper develops a nonlinear VIC that yields the following contributions:

1) A nonlinear VIC formulation is derived based on the objective holographic feedbacks theory (OHFT) [34] and active power modulation scheme. The proposed design improves frequency nadir and suppresses the corresponding drivetrain torsional oscillation of WTG simultaneously. The key idea is to construct the completely controllable Brunovsky system considering the requirements of frequency response and WTG drivetrain torsional oscillation control objectives.

2) The modified time-varying and rotor speed dependent functions are developed to automatically regulate the frequency support power of WTGs considering the variations of wind speed and operating rotor speeds. This facilitates smooth and fast recovery of WTG rotor speed to the original MPP before the disturbance and prevents the secondary frequency dip caused by the sharp switch between frequency support mode and rotor speed recovery mode.

3) The concept of participation factor is extended to adaptively coordinate the distribution of frequency support power among multiple WTGs in terms of enhancing frequency nadir while avoiding the over-deceleration of WTG rotor speed.

B. Organization

The remainder of this paper is organized as follows. Section II introduces the OHFT and existing VIC control strategies and their related issues. The proposed nonlinear VIC is also presented in Section II. Extensive simulations are carried out and analyzed in Section III. Section IV concludes the paper.

II. OHFT-based Nonlinear VIC of WTGs

This section outlines the OHFT, presents the proposed nonlinear VIC control for single WTG, and finally, discusses how to extend such a control to the scenario of multiple WTGs.

A. Objective Holographic Feedbacks Theory

A single-input-multiple-outputs nonlinear system can be described by the follow equations:

$$\begin{aligned} \frac{d\boldsymbol{x}}{dt} &= \boldsymbol{r}(\boldsymbol{x}) + \boldsymbol{s}(\boldsymbol{x})u\,, \\ \boldsymbol{y} &= \boldsymbol{h}(\boldsymbol{x})\,, \end{aligned} \tag{1}$$

where $\boldsymbol{x}$ and $\boldsymbol{y}$ are the state and output vectors, respectively; u is the control input, $\boldsymbol{r}(\boldsymbol{x})$, $\boldsymbol{s}(\boldsymbol{x})$ and $\boldsymbol{h}(\boldsymbol{x})$ are vectors of nonlinear functions. If $[y_1^*, y_2^*, ..., y_m^*]$ are the target output variables, define the following multiple-objective equations

$$I_i = y_i - y_i^* \qquad i = 1, 2, \ldots, m\,, \tag{2}$$

where m is the number of output variables and I_i represents the tracking error of y_i. The following conditions have to be satisfied:

$$\lim_{t\to 0} |I_i| = 0 \qquad i = 1, 2, \ldots, m\,. \tag{3}$$

To achieve (3), we need to find out the output variable with the relative order of 1 to system (1), supposing to be y_m, then one has:

$$\dot{y}_m = L_r h_m(\boldsymbol{x}) + L_s L_r^0 h_m(\boldsymbol{x})u\,, \tag{4}$$

where $L_s L_r^0 h_m(\boldsymbol{x}) \neq 0$ and L is the Lie derivative operator [35]. To this end, the Brunovsky system can be constructed based on (2) as

$$\dot{\boldsymbol{I}} = \boldsymbol{A}\boldsymbol{I} + \boldsymbol{B}v\,, \tag{5}$$

where

$$\boldsymbol{I} = \begin{bmatrix} I_1 \\ I_2 \\ \vdots \\ I_m \end{bmatrix}, \quad \boldsymbol{A} = \begin{bmatrix} 0 & 1 & 0 & \cdots & 0 \\ 0 & 0 & 1 & \cdots & 0 \\ \vdots & \vdots & & \vdots & \vdots \\ 0 & 0 & 0 & \cdots & 1 \\ 0 & 0 & 0 & \cdots & 0 \end{bmatrix}, \quad \boldsymbol{B} = \begin{bmatrix} 0 \\ 0 \\ \vdots \\ 0 \\ 1 \end{bmatrix}.$$

From (4) and (5), v can be expressed as

$$v = L_r h_m(\boldsymbol{x}) + L_s L_r^0 h_m(\boldsymbol{x})u - \dot{y}_m^*\,. \tag{6}$$

Since the Brunovsky system (5) is a completely controllable linear system, the linear control theory, such as linear quadratic optimal control [36] can be applied to obtain v, yielding:

$$v = \sum_{k=1}^{m} -k_i I_i \,. \tag{7}$$

Using (2), (6) and (7), the control strategy of the nonlinear system (1) can be derived as:

$$u = \frac{-\sum_{i=1}^{m} k_i (y_i - y_i^*) - L_r h_m(\boldsymbol{x}) + \dot{y}_m^*}{L_s L_r^0 h_m(\boldsymbol{x})} \,. \tag{8}$$

The interested readers can find more details on the effectiveness of OHFT in [34].

B. System Description

In this section, the WTG model along with the drivetrain rotating mechanism and the active power control loop, the power grid primary frequency regulation model, the conventional VIC scheme and its impacts on driven-train torsional oscillation of WTG are presented and analyzed.

1) Drive-train model of WTG: The two-mass drive-train model of WTG can be expressed as [32]

$$\begin{aligned} 2H_t \frac{d\omega_t}{dt} &= T_m - K_{sh}\theta_{sh} - D_{sh}(\omega_t - \omega_g) \,, \\ 2H_g \frac{d\omega_g}{dt} &= K_{sh}\theta_{sh} + D_{sh}(\omega_t - \omega_g) - T_e \,, \\ \frac{d\theta_{sh}}{dt} &= \omega_B(\omega_t - \omega_g) \,, \end{aligned} \tag{9}$$

where H_t and H_g are the inertia constants of the wind turbine and generator in seconds, respectively; ω_t and ω_g denote the speeds of wind turbine and generator rotor in radians/s, respectively. K_{sh} and D_{sh} represent the stiffness coefficient and the damping coefficient of the shaft, respectively. T_m, T_e and θ_{sh} are mechanical torque, electromagnetic torque of DFIG and torsional angle between the wind turbine and generator rotor, respectively.

According to the law of aerodynamics, the mechanical power extracted by the WTG can be calculated by [37]:

$$\begin{aligned} P_m &= \frac{\pi \rho R^2 V_w^3 C_p(\lambda,\beta)}{2P_{\mathrm{WTGrate}}} \,, \\ \lambda &= \frac{R\omega_t \omega_{\mathrm{WTGrate}}}{V_w} \,, \\ C_p(\lambda,\beta) &= 0.5176(\frac{116}{\lambda_i} - 0.4\beta - 5)e^{\frac{-21}{\lambda_i}} + 0.0068\lambda \,, \\ \frac{1}{\lambda_i} &= \frac{1}{\lambda + 0.08\beta} - \frac{0.035}{\beta^3 + 1} \,, \end{aligned} \tag{10}$$

where ρ, V_w, P_m, λ, β R, $C_p(\lambda,\beta)$, $\omega_{\mathrm{WTGrate}}$ and P_{WTGrate} are the air density, wind speed, mechanical power, tip-speed ratio, pitch angle, rotor radius, power coefficient, nominal value of WTG rotor speed and WTG rated power, respectively.

2) Modeling of WTG active power control loop: This section considers the following conventions: (a) WTG is modeled with a DFIG; (b) all variables are referenced to the stator side of generator; (c) the reference dq frame rotates at synchronous angular speed of ω; (d) the positive power directions of stator and rotor are assumed to be out and into the generator,

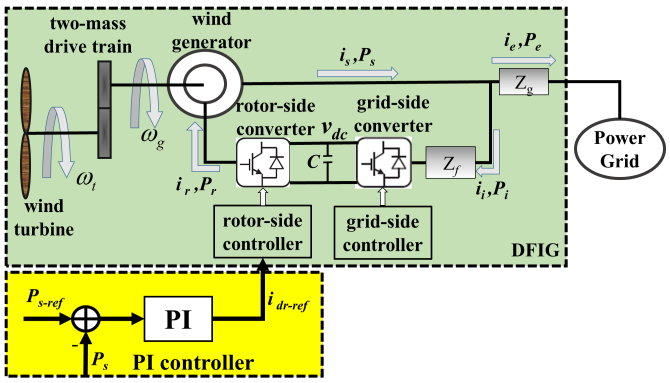

Fig. 1. Schematic diagram of DFIG with two-mass drive train and stator active power control loop

respectively. (11) and (12) show the voltage-flux equations of the stator and rotor, respectively; (13) and (14) present the corresponding flux-current equations, and the active power is given by (15).

$$\begin{aligned} v_{\mathrm{qs}} &= -R_s i_{\mathrm{qs}} + \dot{\psi}_{\mathrm{qs}} - \omega\psi_{\mathrm{ds}} \,, \\ v_{\mathrm{ds}} &= -R_s i_{\mathrm{ds}} + \dot{\psi}_{\mathrm{ds}} + \omega\psi_{\mathrm{qs}} \,, \end{aligned} \tag{11}$$

$$\begin{aligned} v_{\mathrm{qr}} &= R_{\mathrm{r}} i_{\mathrm{qr}} + \dot{\psi}_{\mathrm{qr}} + (\omega - \omega_{\mathrm{g}})\,\psi_{\mathrm{dr}} \,, \\ v_{\mathrm{dr}} &= R_{\mathrm{r}} i_{\mathrm{dr}} + \dot{\psi}_{\mathrm{dr}} - (\omega - \omega_{\mathrm{g}})\,\psi_{\mathrm{qr}} \,, \end{aligned} \tag{12}$$

$$\begin{aligned} \psi_{\mathrm{qs}} &= -L_s i_{\mathrm{qs}} + L_{\mathrm{m}} i_{\mathrm{qr}} \,, \\ \psi_{\mathrm{ds}} &= -L_s i_{\mathrm{ds}} + L_{\mathrm{m}} i_{\mathrm{dr}} \,, \end{aligned} \tag{13}$$

$$\begin{aligned} \psi_{\mathrm{qr}} &= L_{\mathrm{r}} i_{\mathrm{qr}} - L_{\mathrm{m}} i_{\mathrm{qs}} \,, \\ \psi_{\mathrm{dr}} &= L_{\mathrm{r}} i_{\mathrm{dr}} - L_{\mathrm{m}} i_{\mathrm{ds}} \,, \end{aligned} \tag{14}$$

$$\begin{aligned} P_{\mathrm{s}} &= v_{\mathrm{ds}} i_{\mathrm{ds}} + v_{\mathrm{qs}} i_{\mathrm{qs}} \,, \\ P_{\mathrm{r}} &= v_{\mathrm{dr}} i_{\mathrm{dr}} + v_{\mathrm{qr}} i_{\mathrm{qr}} \,, \end{aligned} \tag{15}$$

where v, ψ, R and i represent the voltage, flux, resistance and current, respectively; the subscripts s, r, d, and q denote the stator, rotor, d-axis and q-axis quantities; L_{s} and L_{r} are the corresponding stator and rotor self inductance; L_{m} is the mutual inductance; P_{s} denotes the output active power of DFIG stator; P_{r} is the injected active power into DFIG rotor from the power grid.

In the dq reference frame with the stator voltage orientation, the d-axis is aligned with the stator voltage vector of DFIG. Consequently, u_{qs} is set to zero and $u_{\mathrm{ds}} = U_s$, where U_s is the voltage magnitude of DFIG stator. The active power of DFIG (15) turns into:

$$P_{\mathrm{s}} = \tfrac{3}{2}\tfrac{L_{\mathrm{m}}}{L_{\mathrm{s}}} U_s i_{\mathrm{dr}} \,, P_{\mathrm{r}} = \tfrac{3}{2}\tfrac{L_{\mathrm{m}}}{L_{\mathrm{s}}} U_{\mathrm{s}} i_{\mathrm{dr}} s_l \,, \tag{16}$$

where s_l represents the slip rotor of DFIG. Equation (16) indicates that the output active power of DFIG stator P_{s} can be controlled through the d-axis current of DFIG rotor and the total active power DFIG injects into the grid, denoted by P_e, can be expressed as:

$$P_e = P_{\mathrm{s}} - P_{\mathrm{r}} = P_{\mathrm{s}}(1 - s_l) \,. \tag{17}$$

The schematic diagram of DFIG with two-mass drive train and stator active power control loop is depicted by Fig. 1.

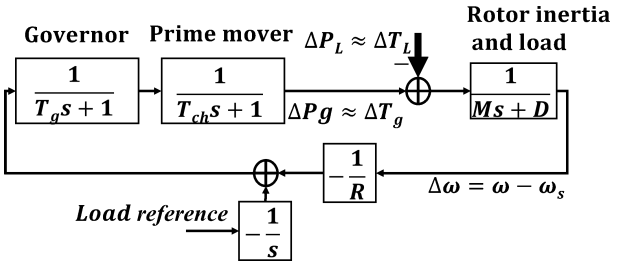

Fig. 2. Block diagram of power grid primary frequency regulation.

Note that, on the basis of [30], the active power control loop of DFIG can be modeled by the following transfer function:

$$P_e = P_{\text{ref}} \frac{\alpha_p}{s+\alpha_p}\,, \tag{18}$$

where α_p is a constant coefficient and P_{ref} denotes the reference electromagnetic power DFIG injects into the grid, which is determined by the MPP tracing strategy [38] given by

$$P_{\text{ref}} = P_{\text{MPP}} = k_{\text{opt}}\omega_g^3\,, \tag{19}$$

where k_{opt} is the MPP tracing coefficient.

3) Conventional VIC of WTG: The conventional VIC for WTG is developed to support the power grid frequency and it determines the reference electromagnetic power increment delivered from WTG to the grid, P_{vir}. Formally, one has

$$P_{\text{vir}} = -k_{P_{\text{vir}}}\Delta\omega - k_{D_{\text{vir}}}\frac{d\Delta\omega}{dt}\,, \tag{20}$$

where $\Delta\omega = \omega - \omega_s$; ω and ω_s denote the angular velocity of power grid and the synchronous angular velocity; $k_{\text{P}_{\text{vir}}}$ and $k_{D_{\text{vir}}}$ are the positive coefficients of the proportional and differential elements, respectively. As a result, the actual reference electromagnetic power of WTG equals to:

$$P_{\text{ref}} = P_{\text{MPP}} + P_{\text{vir}}\,. \tag{21}$$

4) Equivalent model of the grid: The power grid is modeled for simplicity but without loss of generality as an equivalent synchronous generator plus a load [39]. The primary frequency regulation of the power grid is described by the block diagram shown in Fig. 2, where M is the equivalent inertia constant of the grid; D is the frequency coefficient of load that is expressed as percent change in load divided by percent change in frequency; ΔP_L denotes the load variation in the power grid; ΔP_g is the increment of synchronous generator output power; R is the equivalent droop coefficient, the governor and prime mover of the equivalent synchronous generator are treated as inertia elements with time constants T_g and T_{ch}, respectively. Particularly, in the primary frequency regulation, the load reference is usually set as 0. Therefore, we have

$$\frac{d^2\Delta P_g}{dt^2} = \frac{1}{T_g T_{ch}}\Delta\omega - \frac{T_g+T_{ch}}{T_g T_{ch}}\frac{d\Delta P_g}{dt} - \frac{1}{T_g T_{ch}}\Delta P_g\,. \tag{22}$$

As the fluctuation of power grid frequency is small, the corresponding electromagnetic torque approximately equals to the electromagnetic power. Then, considering the variation

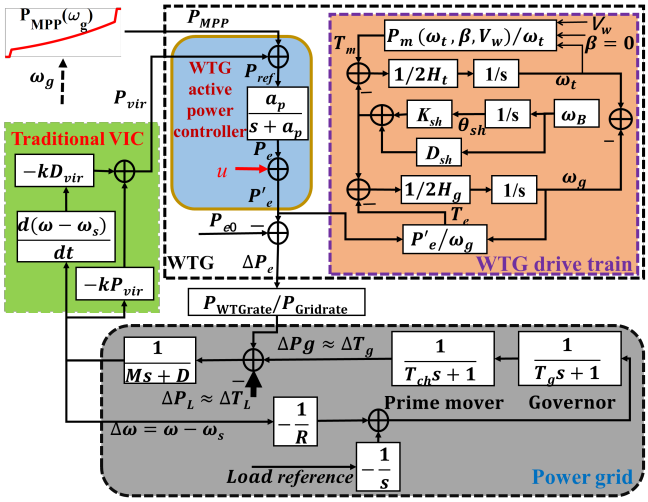

Fig. 3. Block diagram of the whole system.

of WTG output active power, the dynamic equation of the synchronous generator rotor is approximated as:

$$M\frac{d\Delta\omega}{dt} = \Delta P_{\text{tot}} - D\Delta\omega\,, \tag{23}$$

where $\Delta P_{\text{tot}} = \Delta P_g + P_e - P_{e0} - \Delta P_L$ and P_{e0} is the initial output active power of WTG.

5) Drivetrain torsional oscillations of WTG motivated by VIC: The transfer function from the electromagnetic torque increment of WTG, ΔT_e, to the torsional angle variation, $\Delta\theta_{sh}$, can be derived from (9). At the initial moment of frequency event, $\Delta T_e = \frac{P_{\text{vir}}}{\omega_{g0}}$ holds, yielding:

$$\Delta\theta_{sh} = \frac{\omega_B H_t}{2(H_t H_g)s^2 + aH_{tg}s + bH_{tg}}\frac{P_{\text{vir}}}{\omega_{g0}}\,, \tag{24}$$

where $H_{tg} = H_t + H_g$; $a = D_{sh}\omega_B$; $b = K_{sh}\omega_B$ and ω_{g0} denotes the initial WTG rotor speed of MPP before VIC is activated. From (24), we observe that the reference electromagnetic power increment requested by VIC may result in the drivetrain torsional oscillation if no damping control is provided. In fact, there exists a torsional mode with the natural low frequency shown in (25) and the damping coefficient D_{sh} is usually small [31].

$$\omega_n = \sqrt{\frac{\omega_B K_{sh} H_{tg}}{2H_t H_g}}\,. \tag{25}$$

According to the works in [27]–[29], [32], [33], the torsional oscillation frequency of WTG typically lies in [1 2.5] Hz.

The complete system block diagram is reported by Fig. 3, where u is the control input. The power grid and WTG are in pu by their own rated power, i.e., P_{Gridrate} and P_{WTGrate}, respectively. In this paper, the nominal values of angular velocity with respect to power grid and WTG rotor are 120π radians/s and $120\pi/p$ radians/s, respectively, where p represents the number of WTG pole-pairs.

C. Proposed VIC With Single WTG

The state-space description of the whole system can be expressed in the form of (1), where the state variables

are $[\omega_t, \omega_g, \theta_{sh}, P_e, \Delta P_g, \omega]$. This paper aims at designing a nonlinear VIC of WTG, which has the following functions: (i) preventing large frequency excursions of power grid; (ii)suppressing drivetrain torsional oscillations motivated by VIC; (iii) facilitating the smooth and fast recovery of the kinetic energy of the WTG; and (iv) avoiding the secondary frequency dip and drivetrain torsional oscillation of WTG caused by the conventional VIC.

For the former two objectives, based on the aforementioned OHFT, one first chooses ω_{tg} and $\Delta\omega$ as the output variables and derives the following Brunovsky system:

$$\begin{bmatrix} \dot{\omega}_{tg} \\ \Delta\dot{\omega} \end{bmatrix} = \begin{bmatrix} 0 & 1 \\ 0 & 0 \end{bmatrix} \begin{bmatrix} \omega_{tg} \\ \Delta\omega \end{bmatrix} + \begin{bmatrix} 0 \\ 1 \end{bmatrix} v\,, \tag{26}$$

where $\omega_{tg} = \omega_t - \omega_g$. Substituting u into (23) yields

$$M\frac{d\Delta\omega}{dt} = \Delta P_{\rm tot} - D\Delta\omega + u\,. \tag{27}$$

The comparison of (27) and (4) shows that $L_s L_r^0 \Delta\omega = \frac{1}{M} \neq 0$, thus, $\Delta\omega$ is the output with relative order of 1 to the studied system depicted by Fig. 3.

The torsional angle θ_{sh} is the critical quantity to reflect the drivetrain torsional oscillation of WTG. Therefore, along with the frequency response of VIC, the change rate of the WTG torsional angle $d\theta_{sh}/dt$ and the power grid angular frequency ω are required to be close to 0 and 1 pu as possible, respectively. Namely, $d\theta_{sh}/dt = \omega_{tg} = 0$ and $\Delta\omega = \omega - \omega_s = 0$ are the control objectives. These objectives can be achieved by the linear quadratic optimal control, whose performance indicator about system (26) is constituted as follows:

$$J = \int_0^\infty \boldsymbol{I^T Q I} + \alpha v^2 dt\,, \tag{28}$$

where $\boldsymbol{Q}$ is a symmetric positive definite matrix; coefficient α is a positive real number and $\boldsymbol{I} = [\omega_{tg}, \Delta\omega]^T$. According to the control strategy (8) designed by means of OHFT, the nonlinear state feedback control strategy of the targeted system (26) can be obtained by:

$$u = -Mk_1\omega_{tg} - (Mk_2 - D)\Delta\omega - \Delta P_{\rm tot}\,. \tag{29}$$

In this paper, the linear quadratic optimal control is applied to the Brunovsky system (28) to obtain the coefficient k_1 and k_2; D is the frequency coefficient of load that is expressed as percent change in load divided by percent change; $\boldsymbol{Q}$ is used to express the degree of importance for the output variables we are interested in. Here, the grid frequency deviation and the derivative of torsional angle are the interested variables. We put the same weights on them, i.e., $\boldsymbol{Q}$ is an unit matrix.

Converting u into a quantity of the conventional VIC output interface u' yields:

$$u' = u + \frac{1}{a_P}\frac{du}{dt}\,. \tag{30}$$

Combining (30) with the conventional VIC expressed by (20), a nonlinear VIC can be obtained as

$$P'_{\rm vir} = P_{\rm vir} + u'\,. \tag{31}$$

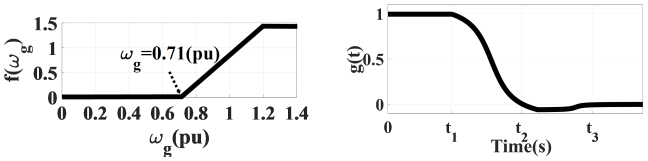

(a) (b)

Fig. 4. (a) Function of rotor speed $f(\omega_g)$; (b) Function of time $g(t)$.

To further satisfy the reference electromagnetic power increment required by VIC, $P'_{\rm vir}$ should be adjusted following the WTG rotor speed ω_g. In other words, VIC requires more power increment at the high rotor speed when there is enough kinetic energy that can be released, and vice versa. Thus, the result of VIC in (31) is multiplied by a function of rotor speed, $f(\omega_g)$, yielding:

$$P''_{\rm vir} = P'_{\rm vir}\, f(\omega_g)\,, \tag{32}$$

where $f(\omega_g)$ is shown in Fig. 4(a).

To achieve the goal of facilitating smooth and fast recovery of WTG rotor speed, a function of time $g(t)$ shown in Fig. 4(b) is multiplied by (32). A positive $g(t)$ promotes WTG to provide active power for frequency support while a negative $g(t)$ is effective in the recovery of WTG rotor speed. Note that $g(t)$ also makes the power for frequency support to vary smoothly. This helps avoid drivetrain torsional oscillations of the WTG and the secondary frequency dip. Finally, the proposed VIC can be given by:

$$P'''_{\rm vir} = P''_{\rm vir}\, g(t) = P'_{\rm vir}\, f(\omega_g)\, g(t)\,. \tag{33}$$

D. Extension to Multiple WTGs

The proposed nonlinear VIC controller is now extended to multiple WTGs. For multiple WTGs, the Brunovsky system can be constructed as

$$\begin{bmatrix} \dot{\omega}_{tg,1} \\ \dot{\omega}_{tg,2} \\ \vdots \\ \dot{\omega}_{tg,N} \\ \Delta\dot{\omega} \end{bmatrix} = \begin{bmatrix} 0 & 1 & 0 & \cdots & 0 \\ 0 & 0 & 1 & \cdots & 0 \\ \vdots & \vdots & & \vdots & \vdots \\ 0 & 0 & 0 & \cdots & 1 \\ 0 & 0 & 0 & \cdots & 0 \end{bmatrix} \begin{bmatrix} \omega_{tg,1} \\ \omega_{tg,2} \\ \vdots \\ \omega_{tg,N} \\ \Delta\omega \end{bmatrix} + \begin{bmatrix} 0 \\ 0 \\ \vdots \\ 0 \\ 1 \end{bmatrix} v\,, \tag{34}$$

where the subscript i denotes the quantities with respect to the ith WTG and N is the number of WTGs.

Similar to the design procedure of single-WTG VIC, the control input u equals to:

$$u = -\sum_{i=1}^{N} Mk_i\omega_{tg,i} - (M\ k_{N+1} - D)\Delta\omega - \Delta P_{tot}\ , \tag{35}$$

where $k_1, k_2, \ldots, k_{N+1}$ represent the state feedback coefficients when applying linear quadratic optimal control for the system (34) to obtain control quantity v; $\Delta P_{\rm tot} = \Delta P_g + \sum_{i=1}^{N}(P_{e,i} - P_{e0,i}) - \Delta P_L$; $P_{e0,i}$ and $P_{e,i}$ denote the initial and real-time active power of the ith WTG, respectively.

Then, the signal $P'''_{\rm vir,tot}$ for multiple WTGs integrated power system is obtained as:

$$P'''_{\rm vir,tot} = \sum_{i=1}^{N} P'_{\rm vir} \cdot {\rm pf}_i \cdot f(\omega_{g,i}) \cdot g(t)\,, \tag{36}$$

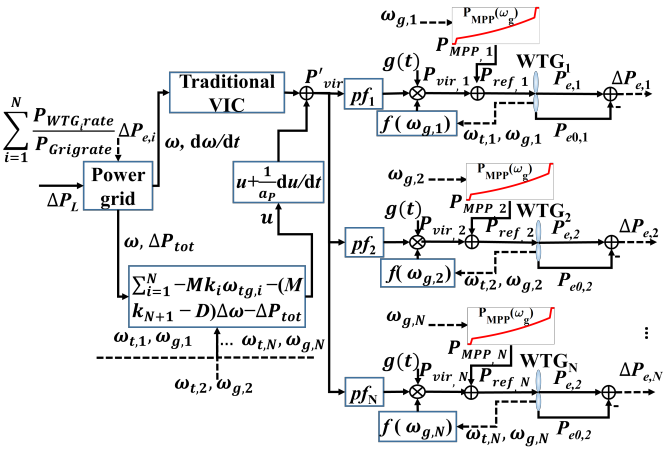

Fig. 5. The block diagram of the proposed nonlinear VIC.

where $P'_{\rm vir}$ can be calculated by (30) and (31) as well. pf_i $(i = 1, 2, \ldots, N)$ represents the participating factor of the ith WTG; note that all power should be converted into quantities in pu by nominal power of the power grid; the participating factor of the ith WTG, pf_i, determines the power support from each WTG and it is correlated with the WTG initial operation point. Formally, one has

$$\mathrm{pf}_i = \frac{P_{e0,i}}{\sum_{i=1}^{k} P_{e0,i}} \qquad i = 1, 2, \ldots, N\,, \tag{37}$$

where the initial active power output of the ith WTG, $P_{e0,i}$, can be calculated based on the power flow solution at the moment of contingency.

By integrating the idea of nonlinear VIC for single WTG with the concept of participation factor used for the power distribution among synchronous generators, the proposed method (36) not only delivers the solution of adaptively coordinating the distribution of frequency support power among multiple WTGs, but also maintaining the benefits of providing VIC. In Fig.5, if $N = 1$, it reduces to the single WTG scenario.

The advantages of the proposed VIC are concluded as: (i) improving the power grid frequency nadir through the dynamic coordination of all WTGs; (ii) effectively suppressing the drivetrain torsional oscillation of each WTG caused by the sudden variation of WTG electromagnetic power requested from VIC, (iii) achieving smooth and fast recovery of each WTG rotor speed to the corresponding original MPP before the disturbance and (iv) preventing the secondary frequency dip and drivetrain torsional oscillation of each WTG caused by the sudden quit of traditional VIC. These benefits will be demonstrated in the simulation results section.

III. Simulation Results

In this section, simulations are carried out to demonstrate the advantages of the proposed VIC. The conventional constant-coefficient VIC presented in (20) and the VIC-I defined by:

$$P''''_{\rm vir} = P_{\rm vir}\, g(t) \tag{38}$$

are used for comparisons. Note that the VIC-I is different from that in [16] with time-varying droop coefficient, i.e., the proportional coefficient. Here, both the proportional and differential coefficients are time-varying in VIC-I. It should be noted that there are thresholds related to the maximum and minimum rotor speeds to avoid the over speed for high wind speed and frequency starting-up and closing-down for low wind speed. In other words, the rotor speed can operate within the range by automatically adjusting the electromagnetic power via the rotor speed-active power control loop.

In the Matlab Simulink, the proposed VIC and its comparisons are tested using simplified system and an electrical power system with detailed models of the components, such as synchronous generator, transformer and wind power plant. $\boldsymbol{Q}$ matrices for system (26) and (34) are all identity matrices with appropriate dimension and $\alpha = 1$. The expression of $g(t)$ shown in Fig. (4(a)) is given as:

$$g\,(t) = \begin{cases} 1 & 0 < t \le t_1 \\ P_{y1} \arctan\left(-P_{x1}\,(t - d_{x1}) + d_{y1}\right) & t_1 < t \le t_1 + d_t \\ P_{y2} \arctan\left(P_{x2}\,(t - d_{x2}) + d_{y2}\right) & t > t_1 + d_t \end{cases} \tag{39}$$

where $d_{x1}, P_{x1}, d_{y1}, P_{y1}, d_{x2}, P_{x2}, d_{y2}, P_{y2}$ and d_t are 32.5, 0.2, 1.1, 0.435, 59, 0.6, $-\frac{\pi}{2}$, 0.02 and 27, respectively.

TABLE I
Parameter Settings of the Simplified-Model Test System

Equivalent power grid			
M	4.584 s	D	1
T_g	0.23 s	R	0.03
ΔP_L	0.2 pu	ω_s	377 rad/s
$P_{\rm Gridrate}$	3 MW	T_{ch}	0.2 s
WTG			
$P_{\rm WTGrate}$	1.5 MW	$\omega_{\rm WTGrate}$	377/3 rad/s
H_g	0.685 s	H_t	4.32 s
$D_{\rm sh}$	1.5	K_{sh}	1.1 pu/rad
$k_{\rm opt}$	0.4425	$\omega_g^{\rm min}$	0.708 pu
$\omega_g^{\rm max}$	1.2 pu	a_P	31.4 rad/s
p	3		
Conventional VIC			
$k_{P_{\rm vir}}$	7	$k_{D_{\rm vir}}$	4
Function $g(t)$			
t_1	20 s	t_2	42 s
t_3	64 s		

A. Simulations with Simplified Model

The simplified model is shown in Fig. 3. The parameters of equivalent power grid, WTG, conventional VIC and $g(t)$ are reported in Table I; the nominal power grid frequency is 60 Hz. It is worth pointing that the active power output increment of WTG, ΔP_e, is the sum of reference electromagnetic power increment according to the MPP tracing strategy shown in (19) and the extra active power required by the VIC, i.e., $\Delta P_e = \Delta P_{\rm MPP} + P_{\rm vir}$. The MPP tracing curve of WTG is presented by Fig. 6 and note that this paper concentrates on the MPP tracing area. Section III-A-1) is used to demonstrate the advantages of proposed VIC with single WTG and its performance under different wind speed scenarios is investigated in Section III-A-2). Results on multiple WTGs integrated system are shown in Section III-A-3). For all simulations, a load contingency with 0.2 pu power increment occurs at 20s in the power grid and the conventional VIC maintains for a preset period of 20s.

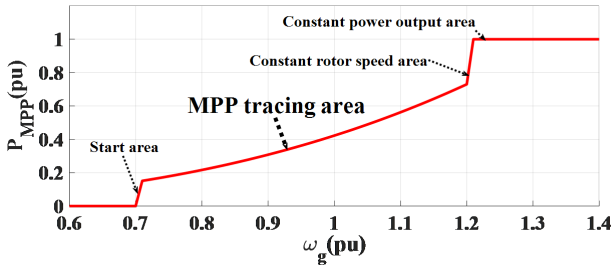

Fig. 6. The MPP tracing curve of WTG.

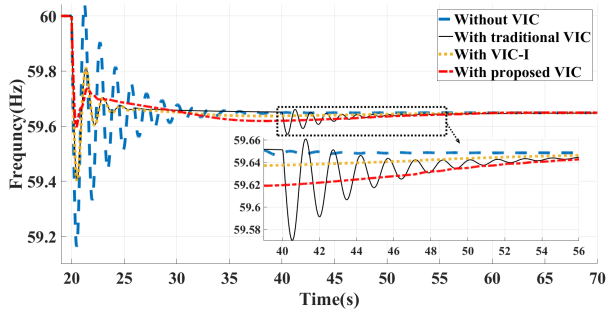

Fig. 7. Frequency response with different VICs for single WTG.

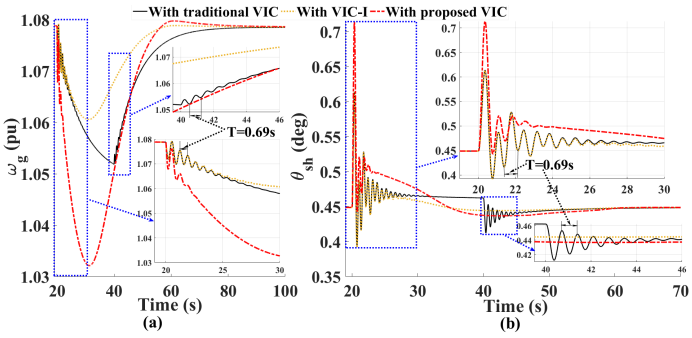

Fig. 8. Rotor speed (a) and torsional angle (b) responses of WTG with different VICs.

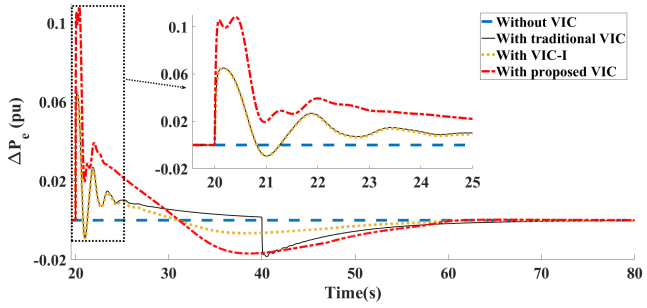

Fig. 9. Active power output increment of WTG with different VICs.

1) VIC for Single WTG: The wind speed is assumed to be 10.8 m/s and the state feedback coefficients of the linear quadratic optimal control for system (26) are k_1=2.6458 and k_2=2.5083. Fig. 7 presents the frequency responses with different VICs, the rotor speed and torsional angle responses of WTG are shown in Fig. 8. Fig. 9 reports the active power output increment of WTG. Note that the wind power penetration rate equals to 33.3% $=P_{\mathrm{WTGrate}}/(P_{\mathrm{Gridrate}}+P_{\mathrm{WTGrate}})$.

According to the results, we can find that the frequency nadir obtained by the proposed VIC is much higher than the conventional VIC and improved VIC-I, see Fig. 7. This is very important as the system frequency needs support for the first few seconds in the presence of contingency, especially for a system with high penetration of renewable energy and being vulnerable to large frequency decline. The reason is that the proposed VIC allows the WTG to reduce rotor speed as much as possible with a much higher speed than others, see Fig. 8(a). This leads to much more active power increment from WTG, see Fig. 9. It is interesting to observe from Fig. 7 that the power grid encountered a secondary frequency dip at 40s if the conventional VIC is used. This results in a sudden reduction in the active power output of WTG, see the negative value of ΔP_e in Fig. 9. By contrast, this is not an issue for the proposed VIC and the modified VIC-I as they can ensure the smooth transformation between frequency support mode and rotor speed recovery mode. As a result, they can avoid the secondary frequency dip and damp the torsional oscillation, see Fig. 8(b) at 40s. However, at the initial moment of contingency, Fig. 8(b) shows that both conventional VIC and the modified VIC-I are subject to WTG drivetrain torsional oscillation with a period of 0.69s (the oscillation frequency is 1.45 Hz) while the proposed VIC can effectively suppress that. Note that the torsional oscillation is due to the sudden variation of WTG active power output as analyzed in (24) and (25). Moreover, from Fig. 8, it is also noted that the WTG rotor speed responses oscillate with the same frequency of the torsional angle, illustrating that the oscillation of the rotor speed response can reflect the drivetrain torsional oscillation of WTG. This explains the oscillation behavior of WTG rotor speed with traditional VIC at the initial moment of rotor speed recovery duration shown in Fig. 8 (a).

The slopes of rotor speed responses in Fig. 8(a) allow conclusing that the proposed VIC has higher recovery rate of WTG rotor kinetic energy than other two methods (note that the proposed method is the fastest one to recover rotor speed to the original MPP before the disturbance and this would become more obvious in the results shown later). In fact, after the main frequency support at about 32s, the proposed VIC prompts WTG to absorb power from grid at an earlier time in contrast to the conventional VIC.

2) VIC for Single WTG with Different Wind Speeds: The proposed VIC is also tested under different wind speeds to demonstrate its robustness to various operating conditions. The following values for the wind speeds are tested: 7.5 m/s, 9.6 m/s and 11.5 m/s. The frequency responses, WTG rotor speed and torsional angle responses of WTG and active power output increment of WTG are displayed in Fig. 10, Fig. 11 and Fig. 12, respectively.

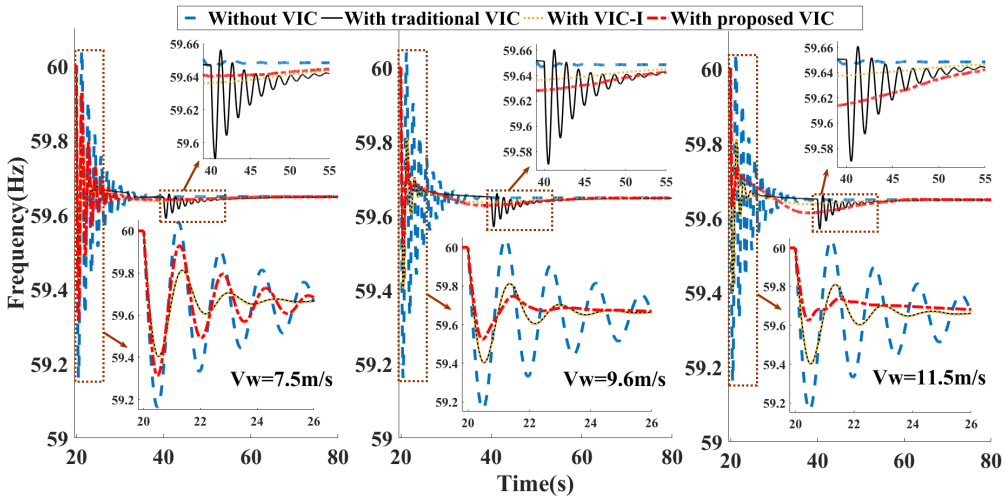

Fig. 10. Frequency responses for different wind speeds.

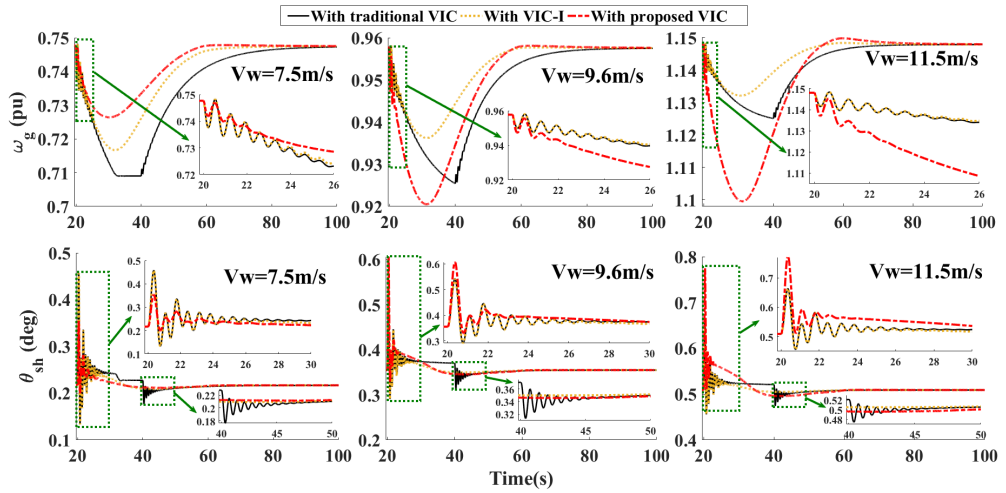

Fig. 11. Rotor speed and torsional angle responses of WTG for different wind speeds.

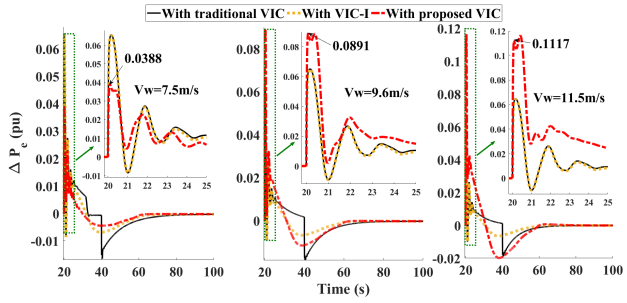

Fig. 12. Active power increment of WTG for different wind speeds.

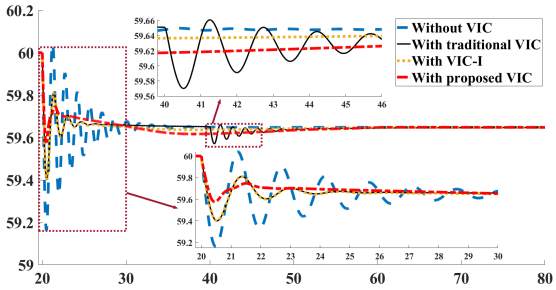

Fig. 13. Frequency responses with multiple WTGs integrated grid.

For the low wind speed scenario, i.e., 7.5 m/s, the first figure of Fig. 11 demonstrates that WTG with proposed VIC releases the smallest kinetic power of WTG rotor, thus providing slightly less active power output increment than the other two methods in the initial stage of frequency regulation, see the first figure of Fig. 12. This results in a slightly lower frequency nadir as shown in the first figure of Fig. 10. It is for the purpose of preventing the reference power of MPP tracing strategy from having a sudden dip to the minimal active power as the rotor speed of WTG reaches the minimal value. Note that there is a rotor speed safeguard measure to guarantee that the rotor speed operates between minimal value 0.708 pu and maximum value 1.2 pu. The rotor speed maintains at the the minimum value until the frequency support mode of VIC ends

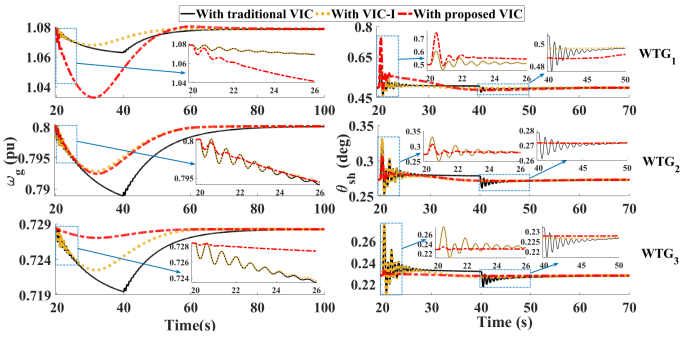

Fig. 14. Rotor speed (left) and torsional angle (right) responses of WTGs with multiple WTGs integrated grid.

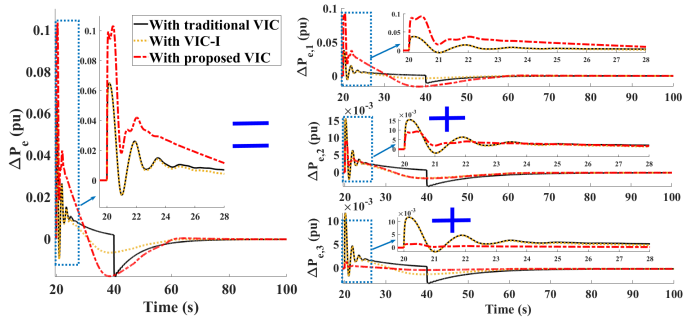

Fig. 15. Active power increment of WTGs with multiple WTGs integrated grid.

and this can explain the WTG rotor speed response in Fig.11 with traditional VIC under 7.5 m/s wind speed. Moreover, the sudden dip of WTG power is encountered by the conventional VIC-based system at 31.46s, see the first figure of Fig. 12. From the torsional angular response of Fig. 11 under 7.5 m/s, it can be found that the comparison methods are still subject to drivetrain torsional oscillation at the initial moment of contingency for VIC-I and the exit time for traditional VIC. This is because of the instantaneous variation of WTG electromagnetic power. The proposed method can effectively suppress that as it can automatically adjust the active power increment of WTG according to the rate of torsional angle.

For higher wind speed scenarios, i.e., 9.6 m/s and 11.5 m/s, the proposed method achieves much better performances in terms of improving the frequency nadir, suppressing the torsional oscillation of WTG, significantly contributing to the smooth and fast recovery of the WTG rotor speed to MPP and effectively avoiding a secondary frequency dip and torsional oscillation of WTG drive train resulted from traditional VIC, see Fig. 10, Fig. 11 and Fig. 12 with respect to 9.6m/s and 11.5m/s of wind speeds. The reason is similar to that in Section III-A-1).

3) VIC for Multiple WTGs Integrated Power Grid: To demonstrate the scalability of the proposed VIC for multiple WTGs, three WTGs with the same parameters as studied in Section III-A-1) are integrated into the power grid. The wind speeds are assumed to be 10.8 m/s, 8 m/s and 7.3 m/s, respectively. The participating factors calculated by (37) are 0.5842, 0.2362 and 0.1796. The state feedback coefficients

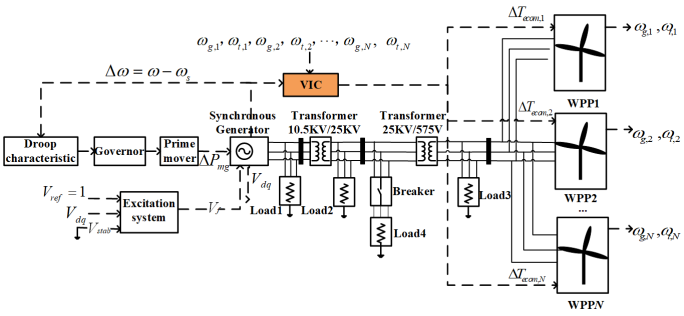

Fig. 16. The diagram of the power system with WPPs integrated.

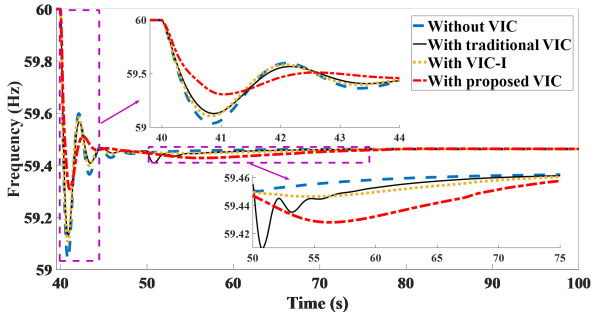

Fig. 17. The frequency response with multiple WPPs integrated power system.

of the linear quadratic optimal control for system (34) are $k_1 = 2.2361$, $k_2 = 5.9389$, $k_3 = 6.7687$ and $k_4 = 3.8128$. Note that the wind power penetration rate is 60% at this time. Comparing results about frequency responses, rotor speed and torsional angle responses of WTGs and active power output increments of WTGs are shown in Figs. 13-15, respectively.

4) VIC for Multiple WPPs Integrated Electrical Power System: These results lead us to draw similar conclusions as for the cases discussed in the previous simulations. They are summarized as follows:

(i) The proposed VIC can achieve better frequency nadir while avoiding the secondary frequency dip, see Fig. 13.

(ii) The proposed VIC effectively suppresses drivetrain torsional oscillation of each WTG caused by the active power output variation requested by VIC, see the initial moment of the rotor speed response with respect to each WTG in Fig. 14 for example. On the other hand, all torsional angle responses of traditional VIC exhibit the torsional oscillations at the initial moment of the speed recovery. The conventional VIC, in fact, stops suddenly to support the frequency and this leads to the instantaneous variation of WTG electromagnetic power.

(iii) The proposed VIC facilitates the fast and smooth recovery of WTG rotor speed, see figures in Fig. 14 for example. From the left figures in Fig. 14, it is interesting to observe that, for WTG1 with higher wind speed, the released rotor kinetic energy with the proposed VIC is larger than the conventional VIC and VIC-I in the initial duration of frequency support mode. By contrast, less reductions in rotor speeds of WTG2 and WTG3 with low wind speeds are observed, which are expected. As a result, WTG1 results in larger active power output increment while those of WTG2 and WTG3 are smaller, see the right figures of Fig. 15. However, the proposed VIC

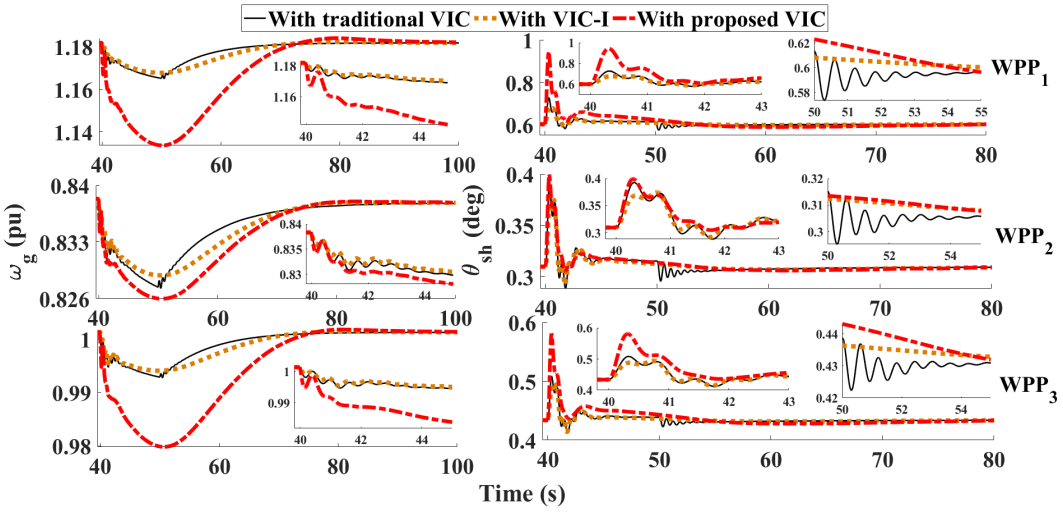

Fig. 18. Rotor speed and torsional angle responses of WPPs with multiple WPPs integrated power system.

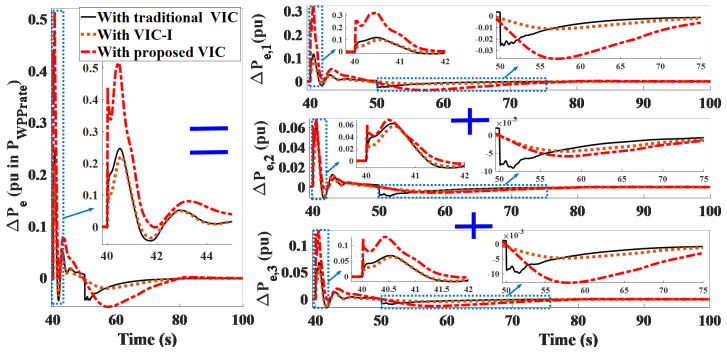

Fig. 19. Active power increments of WPPs with multiple WPPs integrated power system.

can still provide the most total power for frequency support as reported by the left figure of Fig. 15, to achieve the highest frequency nadir. This figure shows that the coordination of multiple WTGs can be effectively and adaptively done by the proposed VIC while the comparisons fail to.

B. Simulations with Detailed Model

To further validate the feasibility and advantages of the proposed VIC, different VICs are tested in a power system with wind power plants (WPPs). The system is shown in Fig. 16, where $\Delta T_{ecom,i}$, $i = 1, 2, \ldots, N$, represents the demanded torque of each WPP requested by VIC and can be calculated by $\frac{P'_{\text{vir}} \cdot \text{pf}_i \cdot f(\omega_{g,i}) \cdot g(t)}{\omega_{g,i}}$; each WPP is treated as an aggregated WGT model with 1.5MW rated power for each DFIG.

In this test, three WPPs are integrated into the power system and each WPP consists of 8 DFIGs, yielding $P_{\text{WTG rate}} = 12$ MW. The wind power penetration is 44.4%. The parameters of synchronous generator, WPPs, loads, conventional VIC and function $g(t)$ are given in Table II. The rated power of synchronous generator is 45 MW. Loads 1-4 are equal to 2 MW, 25 MW, 500 kW and 15 MW, respectively. The corresponding wind speeds of WPPs 1-3 are assumed to be 11.2 m/s, 8 m/s and 9.5 m/s, respectively. Load 4 is connected to the system at 40 s and the conventional VIC maintains for a preset period of 10 s. Other parameters are the same as the previous simulations. The results are shown in Figs. 17-19.

These figures show that the general conclusions are consistent with those using a simplified model in Section III-A. They include (i) improving the power grid frequency nadir; (ii) effectively suppressing the drivetrain torsional oscillation of each WPP caused by the sudden variation of WPP electromagnetic power requested from VIC; (iii) achieving smooth and fast recovery of each WPP rotor speed to the corresponding original MPP before the disturbance; (iv) preventing the secondary frequency dip and drivetrain torsional oscillation of each WPP caused by conventional VIC implementations.

TABLE II
PARAMETER SETTINGS OF THE ELECTRICAL POWER SYSTEM

Synchronous generator			
M	4.56 s	T_g	1 s
T_{ch}	0.2 s	R	0.03
ω_s	377 rad/s	P_{Gridrate}	15 MW
R_s	0.03 pu	x_{d}	1.305 pu
x'_{d}	0.296 pu	x''_{d}	0.252 pu
x_{q}	0.474 pu	x'_{q}	0.243 pu
x''_{q}	0.18 pu		
WPP			
P_{WTGrate}	$1.5 * 8$ MW	ω_{WTGrate}	377/3 rad/s
H_g	0.685 s	H_t	4.32 s
D_{sh}	1.5	K_{sh}	1.1 pu/rad
p	3	R_{s}	0.023 pu
L_{s}	0.18 pu	L_{m}	2.9 pu
R_{r}	0.016 pu	L_{r}	0.16 pu
Loads			
$Load_1$	2 MW	$Load_2$	12 MW
$Load_3$	500 kW	$Load_4$	6 MW
Conventional VIC			
$k_{P_{\text{vir}}}$	7	$k_{D_{\text{vir}}}$	4
Function $g(t)$			
t_1	40 s	t_2	62 s
t_3	84 s		

IV. Conclusions and Future work

This paper develops an OHFT-based nonlinear virtual inertia control of wind power integrated power system. It is able to provide primary frequency support of the power grid by means of releasing the kinetic energy of WTG rotor speed and, in the meanwhile, overcome several limitations of existing VIC methods. Its advantages are concluded as: (i) it can significantly improve the frequency nadir at the initial moment of contingency, enhancing the security and stability of power system; (ii)it suppresses the drivetrain torsional oscillation of WTG resulted from its electromagnetic power variation for the grid frequency support, leading to the enhancement of the service life of WTG; (iii) after frequency support, it achieves fast and smooth recovery of rotor speed to the original MPP before the disturbance; and (iv) it can effectively prevent the secondary frequency dip and drivetrain torsional oscillation of WTG casued by the conventional VIC.

Future work will focus on extending the OHFT-based control for frequency support using multiple distributed energy resources, such as energy storage, PVs, etc.

References

[1] A. Baggini, "*Handbook of Power Quality*," New York: Wiley, 2008.

[2] M. Tsili, S. Papathanassiou, "A review of grid code technical requirements for wind farms," *IET Renew. Powe.r Gen.*,vol. 3, no. 3, pp. 308–332, 2009.

[3] "Eirgrid Grid Code, Version 5.0, Eirgrid, 2012 [Online]. Available: http://www.eirgrid.com/operations/gridcode/."

[4] "Transmission Provider Technical Requirements for the Connection of Power Plants to the Hydro-Québec Transmission System, Hydro-Québec, 2009 [Online]. Available: http://www.hydroquebec.com/transenergie/fr/commerce/raccordement_transport.html."

[5] G. Ramtharan, J. B. Ekanayake, N. Jenkins, "Frequency support from doubly fed induction generator wind turbines," *IET Renew. Power Gen.,*, vol. 1, no. 1, pp. 3–9, 2007.

[6] Z. S. Zhang, *et al.*, "Coordinated frequency regulation by doubly fed induction generator-based wind power plants," *IET Renew. Power Gen.,*, vol. 31, no. 5, pp. 3414–3423, 2016.

[7] R. G. de Almeida, J. A. P. Lopes, "Participation of doubly fed induction wind generators in system frequency regulation," *IEEE Trans. Power Syst.,*, vol. 22, no. 3, pp. 944–950, 2007.

[8] L. R. Chang-Chien, W. T. Lin, Y. C. Yin, "Enhancing frequency response control by DFIGs in the high wind penetrated power systems," *IEEE Trans. Power Syst.,*, vol. 26, no. 6, pp. 710-718, 2011.

[9] J. Ekanayake, N. Jenkins, "Comparison of the response of doubly fed and fixed-speed induction generator wind turbines to changes in network frequency," *IEEE Trans. Energy Convers,*, vol. 19, no. 4, pp. 800–802, 2004.

[10] T. K. Chau, *et. al*, "A novel control strategy of DFIG wind turbines in complex power systems for enhancement of primary frequency response and LFOD," *IEEE Trans. Power Syst.,*, vol.32, no.5, pp.1811-1823, 2018.

[11] P. K. Keung, P. Li, H. Banakar, B. T. Ooi, "Kinetic energy of wind-turbine generators for system frequency support," *IEEE Trans. Power Syst.,*, vol. 24, no. 1, pp. 279–287, 2009.

[12] I. D. Margaris, *et. al.*, "Frequency control in autonomous power systems with high wind power penetration," *IEEE Trans. Sustain. Energy,*, vol. 3, no. 2, pp. 189–199, 2012.

[13] D. Ochoa, S. Martinez, "Fast-frequency response provided by DFIG-wind turbines and its impact on the grid," *IEEE Trans. Power Syst,* vol. 32, no. 5, pp.4002-4011, 2017.

[14] H. T. Ma, B. H. Chowdhury, "Working towards frequency regulation with wind plants: combined control approaches," *IET Renew. Power Gen.,* vol. 4, no. 4, pp. 308-316, 2010.

[15] D. Yang, *et. al*, "Temporary frequency support of a DFIG for high wind power penetration," *IEEE Trans. Power Syst,* vol. 33, no. 3, pp. 3428-3437, 2018.

[16] M. Garmroodi, G. Verbic, D. Hill, "Frequency support from wind turbine generators with a time variable droop characteristic," *IEEE Trans. Sustain. Energy,* vol. 9, no. 2, pp. 676–684, 2018.

[17] J. Morren, S. W. de Haan, W. L. Kling, J. Ferreira, "Wind turbines emulating inertia and supporting primary frequency control," *IEEE Trans. Power Syst.,* vol. 21, no. 1, pp. 433–434, 2006.

[18] J. Morren, J. Pierik, S. W. de Haan, "Inertial response of variable speed wind turbines," *Elect. Power Syst. Res.,* vol. 76, pp. 980–987, 2006.

[19] J. M. Mauricio, A. Marano, A. Gomez-Exposito, J. L. M. Ramos, "Frequency regulation contribution through variable-speed wind energy conversion systems," *IEEE Trans. Power Syst.,* vol. 24, no. 1, pp. 173–180, 2009.

[20] K. V. Vidyanandan, N. Senroy, A. Gomez-Exposito, J. L. M. Ramos, "Primary frequency regulation by deloaded wind turbines using variable droop," *IEEE Trans. Power Syst.,* vol. 28, no. 2, pp. 837-846, 2013.

[21] M. Hwang, *et al.*, "Dynamic droop–based inertial control of a doubly-fed induction generator," *IEEE Trans. Sustain. Energy,* vol. 7, no. 3, pp. 924-933, 2016.

[22] D. Gautam, *et. al.*, "Control strategy to mitigate the impact of reduced inertia due to doubly fed induction generators on large power systems," *IEEE Trans. Power Syst.,* vol. 26, no. 1, pp. 214-224, 2011.

[23] M. Kayikci, J. Milanovic, " Dynamic contribution of DFIG-based wind plants to system frequency disturbances," *IEEE Trans. Power Syst.,* vol. 24, no. 2, pp. 859–867, 2009.

[24] H. Ye, W. Pei, Z. Qi, "Analytical modeling of inertial and droop responses from a wind farm for short-term frequency regulation in power systems," *IEEE Trans. Power Syst.,* vol. 31, no. 5, pp. 3414-3423, 2016.

[25] M. Hwang, *et al*, "Disturbance-adaptive short-term frequency support of a DFIG associated with the variable gain based on the ROCOF and rotor speed," *IEEE Trans. Power Syst.,* vol.32, no.3, pp.1873-1881, 2017.

[26] J. B. Xi, H. Geng, X. Zou, "Decoupling scheme for virtual synchronous generator controlled wind farms participating in inertial response," *J. Mod Power Syst. Cle.,* 2020.

[27] X. Xi, *et. al.*, "Two-Level damping control for DFIG-based wind farm providing synthetic inertial service," *Ind. Appl.,* vol. 54, no. 2, pp. 1712–1723, 2018.

[28] H. Geng, D. Xu, B. Wu, and G. Yang, "Active damping for PMSG based WECS with DC link current estimation," *IEEE Trans. Ind. Electron.,* vol. 58, no. 4, pp. 1110–1119, 2011.

[29] J. Licari, C. E. Ugalde-Loo, J. B. Ekanayake, N. Jenkins, "Damping of torsional vibrations in a variable-speed wind turbine," *IEEE Trans. Energy Convers.,* vol. 28, no. 1, pp. 172–180, 2013.

[30] G. Mandic, A. Nasiri, E. Muljadi, F. Oyague, "Active torque control for gearbox load reduction in a variable-speed wind turbine," *IEEE Trans. Ind. Appl.,* vol. 48, no. 6, pp. 2424–2432, 2012.

[31] M. Rahimi, "Improvement of energy conversion efficiency and damping of wind turbine response in grid connected DFIG based wind turbines," *Int. J. Elec. Power,* vol. 95, pp. 11-25, 2018.

[32] H. Geng, *et al.*, "Hybrid modulated active damping control for DFIG-based wind farm participating in frequency response," *IEEE Trans. Energy Convers.,* vol. 32, no. 3, pp. 1220-1230, 2017.

[33] X. Z. Xi, H. Geng, G. Yang, "Torsional oscillation damping control for DFIG-based wind farm participating in power system frequency regulation," *IEEE Trans. Ind. Appl.,* vol. 54, no. 6, pp. 3687-3701, 2018.

[34] L. Hui, W. Ni, W. Hua, X. Li, "Nonlinear excitation control with objective holographic feedbacks," *Adv. Math.,* vol. 218, no. 4, pp. 1–7, 2008.

[35] E. Reithmeier, "*Nonlinear Dynamics in Engineering Systems*," Springer-Verlag, 1990.

[36] R. Perez-Ibacache, C. Silva, A. Yazdani, " Linear state-feedback primary control for enhanced dynamic response of AC microgrids," *IEEE Trans. Smart Grid,* vol. 10, no. 3, pp. 3149–3161, 2019.

[37] C. Bhende, C. Pradhan, " Frequency sensitivity analysis of load damping co-efficient in wind farm integrated power system," *IEEE Trans. Power Syst.,* vol. 32, no. 2, pp. 1016–1029, 2017.

[38] Z. Chen, M. Yin, Y. Zou, K. Meng, Z. Dong, "Maximum wind energy extraction for variable speed wind turbines with slow dynamic behavior," *IEEE Trans. Power Syst.,* vol. 32, no. 4, pp. 3321–3322, 2017.

[39] L. Grigsby, "*Power system stability and control*", third edition, CRC, 2012.

[40] M. S. El-Moursi, B. Bak-Jensen, M. H. Abdel-Rahman, "Novel STATCOM controller for mitigating SSR and damping power system oscillations in a series compensated wind park," *IEEE Trans. Power Elec.,* vol. 25, no. 2, pp. 429-441, 2010.